Journal of Physiology (1993), **469**, *pp.* 291–313
With 10 figures
Printed in Great Britain

TWO KINETICALLY DISTINCT COMPONENTS OF HYPERPOLARIZATION-ACTIVATED CURRENT IN RAT SUPERIOR COLLICULUS-PROJECTING NEURONS

BY JOEL S. SOLOMON AND JEANNE M. NERBONNE*

From the Department of Molecular Biology and Pharmacology, Washington University School of Medicine, St Louis, MO 63110, USA

(*Received 13 July 1992*)

SUMMARY

1. Whole-cell and perforated patch recording techniques were used to examine the activation, deactivation and inactivation of the time-dependent hyperpolarization-activated inward currents (I_h) in isolated superior colliculus-projecting (SCP) neurons from rat primary visual cortex.

2. Examination of inward current waveforms revealed the presence of two kinetically distinct components of I_h: one that activates with a time constant of the order of hundreds of milliseconds, and one that activates with a time constant of the order of seconds. We have termed these $I_{h,f}$ and $I_{h,s}$, to denote the fast and slow components, respectively, of current activation. The time constants of activation of both $I_{h,f}$ and $I_{h,s}$ decrease with increasing membrane hyperpolarization.

3. Following the onset of hyperpolarizing voltage steps, a delay is evident prior to time-dependent inward current activation. This delay is voltage dependent and decreases with increasing membrane hyperpolarization.

4. The sigmoidal inward current waveforms are well fitted by the sum of two exponentials in which the faster term, corresponding to the activation of $I_{h,f}$, is raised to the power $1{\cdot}34 \pm 0{\cdot}26$ (mean $\pm$ S.D.). The non-integral exponent suggests that $I_{h,f}$ activation involves at least two energetically non-equivalent gating transitions prior to channel opening.

5. Over a limited voltage range, tail currents could also be resolved into two distinct components. The faster component, which corresponds to the deactivation of $I_{h,f}$, decayed over a single exponential time course with a mean ($\pm$S.D.) time constant of 355 ± 161 ms at -70 mV. $I_{h,s}$ decay also followed a single exponential time course with a mean ($\pm$S.D.) time constant of 2428 ± 1285 ms at -70 mV. Both deactivation time constants decreased with increasing depolarization.

6. The separation of inward current activation and deactivation into two distinct components and the lack of correlation between the relative amplitudes of these components suggest that $I_{h,f}$ and $I_{h,s}$ reflect the presence of two functionally distinct channel populations.

7. No decrements in time-dependent hyperpolarization-activated inward currents

* To whom correspondence should be addressed.

were observed during hyperpolarizations lasting up to 18 s, suggesting that neither $I_{h,f}$ nor $I_{h,s}$ inactivates from the open state. In addition, 10 s depolarizations to 0 mV prior to activation did not alter the waveforms of the inward currents activated directly from −40 mV, suggesting that $I_{h,f}$ and $I_{h,s}$ also do not inactivate from closed states.

8. The hyperpolarization-activated currents in rat SCP neurons are ideally suited to contribute to the control of the resting membrane potential and input resistance. Furthermore, the time-dependent properties of $I_{h,f}$ and $I_{h,s}$ may lead to the generation of complex firing patterns such as the rebound firing of action potentials following synaptic inhibition, as well as contribute to the generation and maintenance of rhythmic firing.

INTRODUCTION

Electrical recordings in the mammalian cortex have demonstrated distinct action potential firing patterns attributed to intrinsic differences in the membrane properties of cortical neurons (for review see Connors & Gutnick, 1990). For example, some layer V cells fire action potentials in 'bursts'; whereas, other cells in this layer are classified as 'regular spiking' or 'fast spiking' (Connors, Gutnick & Prince, 1982; McCormick, Connors, Lighthall & Prince, 1985; Chagnac-Amitai, Luhmann & Prince, 1990; Connors & Gutnick, 1990; Mason & Larkman, 1990). These electrophysiological phenotypes undoubtedly reflect variations in the expression of distinct membrane conductance molecules in different cortical cell types. This principle has been elegantly illustrated in studies of thalamic relay neurons where it has been demonstrated that changes in the relative contributions of distinct conductance pathways underlie the switch from rhythmic burst firing to single spiking (McCormick & Pape, 1990). Rhythmic burst firing of thalamic relay neurons relies on an interplay between a hyperpolarization-activated 'pacemaker' current termed, I_h, and a low-threshold calcium current termed, I_T (McCormick & Pape, 1990). For example, at membrane potentials between −70 and −85 mV, activation of I_h depolarizes the cell to the threshold for activation of I_T. Activation of I_T then leads to a 'burst', consisting of multiple sodium-dependent action potentials riding on top of a low-threshold calcium spike. As the calcium channels inactivate, the cell repolarizes and the process repeats. When these cells are depolarized to approximately −60 mV, burst firing is replaced by single spiking as a result of the voltage-dependent inactivation of I_T and the lack of activation of I_h.

Similar analysis of the membrane conductance pathways underlying the distinct firing properties of cerebral cortical neurons has been particularly challenging due, in large part, to the extraordinary cellular diversity in the cortex. Nevertheless, several investigations have focused on examining the membrane properties of different *types* of cortical neurons, identified based on their anatomical connections (Giffin, Solomon, Burkhalter & Nerbonne, 1991) or morphologies (McCormick *et al.* 1985; Chagnac-Amitai *et al.* 1990; Mason & Larkman, 1990). Recently, we have reported (Giffin *et al.* 1991; Solomon & Nerbonne, 1993) the use of an *in vivo* retrograde labelling technique to allow the *in vitro* identification of an anatomically and morphologically uniform subpopulation of layer V visual cortical neurons that project to the superior colliculus (Schofield, Hallman & Lin, 1987; Hallman,

Schofield & Lin, 1988). Using this approach, we have examined the hyperpolarization-activated currents, I_h, in superior colliculus-projecting (SCP) cells (Solomon & Nerbonne, 1993). In SCP neurons, I_h is a mixed sodium and potassium current that begins to activate near -60 mV and is similar, in several respects, to a number of previously described hyperpolarization-activated currents in other systems (Solomon & Nerbonnne, 1993). These studies also revealed that the slow depolarizing *sag* during hyperpolarizing current injections (Mason & Larkman, 1990) in SCP cells results from the time-dependent activation of I_h (Solomon & Nerbonne, 1993). Deactivation of I_h is also responsible for a transient *overshoot* of the resting membrane potential (Mason & Larkman, 1990) following the offset of a maintained hyperpolarizing input (Solomon & Nerbonne, 1993).

Here, we demonstrate that the hyperpolarization-activated currents in SCP neurons comprise two kinetically distinct inward current components that we have termed $I_{h,f}$ and $I_{h,s}$ to denote the fast and slow components, respectively, of inward current activation. Analyses of current activation revealed that the gating of $I_{h,f}$ contrasts with traditional models of voltage-activated channel gating in that it cannot be described adequately by a Hodgkin & Huxley type reaction sequence involving multiple identical closed-state transitions. Rather, the data suggest that $I_{h,f}$ channels traverse at least two energetically non-equivalent transitions prior to opening. In addition, our results suggest that $I_{h,f}$ and $I_{h,s}$ reflect the activation of two functionally distinct ion channel populations.

METHODS

Identification and isolation of projection neurons

Voltage clamp recordings were obtained from SCP neurons identified *in vitro* following *in vivo* retrograde labelling with rhodamine-conjugated latex 'beads' (Katz, Burkhalter & Dreyer, 1984; Thong & Dreher, 1986) according to methods previously described (Solomon & Nerbonne, 1993). Briefly, postnatal day 4–6 Long–Evans rat pups were anaesthetized with 1% halothane–99% air, and beads were pressure injected into the left superior colliculus at one to three sites. Following scalp suturing, animals were allowed to recover from anaesthesia before being returned to the mother. After allowing about 24 h for retrograde bean transport, animals were killed by cervical dislocation (see below), and bead-containing SCP neurons were identified in dissociated cultures of the ipsilateral area 17 under epifluorescence optics (see below). The locations of the injection sites were verified by visual inspection.

For the preparation of dissociated cell cultures, postnatal day 5–15 animals were killed by rapid cervical dislocation and the brains were rapidly removed. Labelled primary visual cortex was isolated and dissociated using slight modifications (Giffin *et al.* 1991; Solomon & Nerbonne, 1993) of previously published procedures (Huettner & Baughman, 1986). Cells were suspended in minimal essential medium (MEM) supplemented with glutamine, penicillin/streptomycin, and heat-inactivated horse serum, plated on monolayers of cortical astrocyte 'feeder layer' cultures (Raff, Fields, Hakomori, Mirsky, Pruss & Winter, 1979) at a density of $\approx 1{\cdot}5 \times 10^5$ cells/ml, and maintained in a humidified air–CO_2 (95%–5%) incubator at 37 °C. Isolated SCP neurons were identified *in vitro* under epifluorescence optics.

Electrophysiological recordings

Electrophysiological recordings were obtained from SCP neurons within the first 48 h after isolation using either the whole-cell (Hamill, Marty, Neher, Sakmann & Sigworth, 1981) or the nystatin perforated patch (Horn & Marty, 1988) recording technique. SCP cells, identified under epifluorescence illumination, were visualized under phase contrast illumination on an inverted microscope (Nikon, USA) at 400×. Cells with minimal process outgrowth were selected for

recordings to ensure adequate spatial control of the membrane voltage (see below). Recordings were obtained from bead-labelled neurons at room temperature (20–22 °C) using a Dagan 8900 patch clamp amplifier (Dagan, USA) with 1 GΩ feedback resistor. Current signals were filtered on line at 2 kHz with an 8-pole Bessel filter (Frequency Devices, USA) and stored on IBM-AT computer using a Tecmar Labmaster interface and pCLAMP data acquisition software (Axon Instruments, USA). Recording pipettes were drawn on a two-stage puller from either soda lime (Kimble 73811) or borosilicate (Boralex) glass capillary tubes. Tip diameters were typically 1 μm. Pipettes were coated with Sylgard to within 5–10 μm of the tip, heat-polished and stored in a closed container until used.

Pipette-membrane seals were ⩾ 8 GΩ. Following series resistance (R_{ser}) compensation, R_{ser} was ⩽ 7 MΩ for whole-cell recordings and ⩽ 22 MΩ for nystatin recordings (Solomon & Nerbonne, 1993). Thus, voltage errors ($R_{ser} \times I_{max}$) were often less than 1 mV and always less than 4·5 mV (Solomon & Nerbonne, 1993). The contents of the intracellular and extracellular recording solutions are listed in Table 1. All experiments, unless otherwise indicated, were conducted in Block bath solution (see Table 1). For whole-cell recordings, the free calcium concentration in the pipette solution was buffered to 100 nM by titrating 10 mM ethyleneglycol-bis-(β-aminoethyl ether)-*N*,*N*,*N*′,*N*′-tetraacetic acid (EGTA) with $CaCl_2$. Bath solution containing caesium chloride was applied by pressure ejection from a glass pipette with a 2–4 μm tip diameter positioned approximately 5–15 μm from the surface of cell being examined.

Data analysis

Data were analysed using pCLAMP, NFIT (Island Products, USA), *Excel* (Microsoft, USA), and CSS: Statistica (StatSoft, USA) software. Summarized data are expressed as mean ± S.D. unless otherwise indicated. Statistical significance was set at the $P < 0{\cdot}05$ level. Whole-cell membrane capacitances were determined by integrating the current records obtained on ±10 mV steps from a holding potential of −60 mV.

In each cell, the quality of spatial voltage control was determined by fitting the capacitance transient decay following ±10 mV steps from a holding potential of −60 mV to an exponential expression of the form:

$$I_{decay} = A_0 + A_1 \exp(-t/\tau_{clamp_1}) + A_2 \exp(-t/\tau_{clamp_2}), \quad (1)$$

where A_ns are free parameters, t is time, and τ_{clamp_n} are the time constants of exponential decay. Cells well described by single exponential capacitative current decays (i.e. decays well fitted with A_2 set equal to zero) were considered adequately clamped, and only data obtained from such cells were analysed further (Lindau & Neher, 1988).

For kinetic analyses in which the data were fitted to expressions defined in the text, correlation coefficients were determined to assess the quality of the fits. In all cases, however, best fits to the experimental data were determined by eye. In addition, arrows have been included in several of the figures pointing to regions of the curve that were defined as not well fitted (by eye). See, for example, Figs 2*A*, 3*F* and 6.

Materials

Pregnant Long–Evans rats were obtained from Harlan Sprague Dawley (Indianapolis, IN, USA). MEM was obtained from Gibco (Grand Island, NY, USA), horse serum from Hyclone (Logan, UT, USA) and papain from Worthington (Freehold, NJ, USA). Sylgard is a product of Dow-Corning (Midland, MI, USA). Rhodamine beads (Lumafluor) were generously provided by Dr Andreas Burkhalter, Washington University. All other reagents were purchased from Sigma Chemical Company Ltd. Kimble glass capillary tubes were obtained from VWR Scientific (Chicago, IL, USA), and Boralex capillaries from Rochester Scientific (Rochester, NY, USA).

RESULTS

Kinetics of inward current activation

Voltage clamp currents recorded in SCP neurons during hyperpolarizing voltage steps to potentials negative to −60 mV comprise an instantaneous current, I_{inst}, followed by the slow activation of the time-dependent current, I_h (Solomon &

Nerbonne, 1993). Initial experiments suggested that the rising phase of I_h in SCP neurons was well described by single exponentials over the entire voltage range of current activation (Fig. 1*A*). Time constants for inward current activation were of the order of hundreds of milliseconds and decreased with increasing hyper-

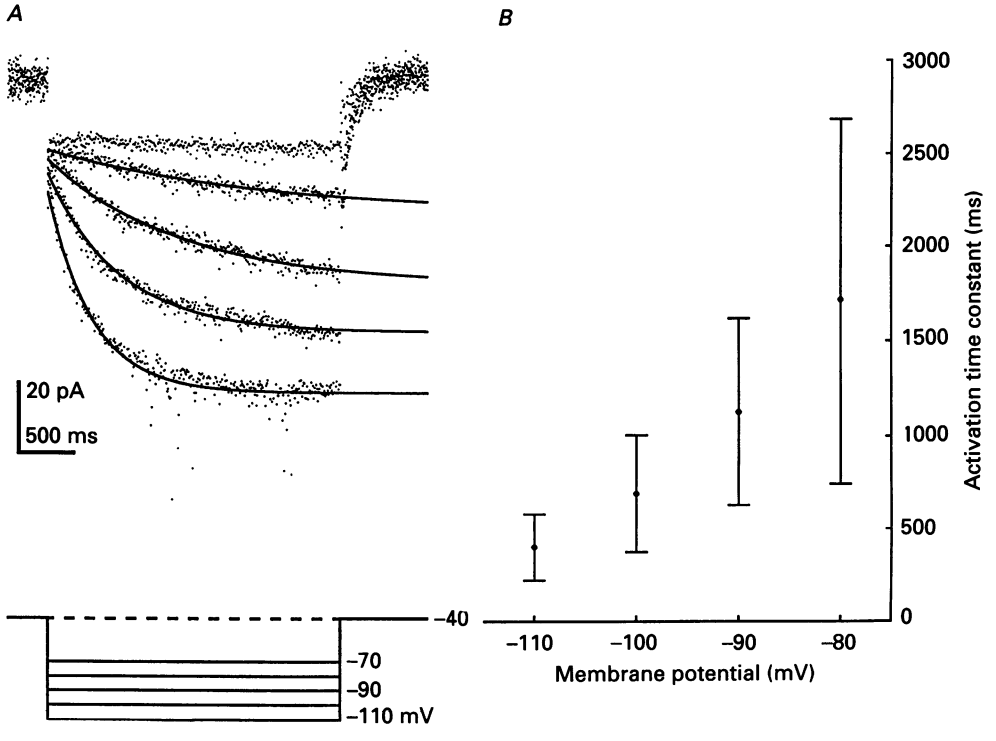

Fig. 1. Inward current activation is approximated by a single exponential. *A*, whole-cell recordings of hyperpolarization-activated inward currents (points) in an SCP neuron evoked during 2·5 s hyperpolarizing voltage steps to potentials between −70 and −110 mV from a holding potential of −40 mV. The current waveforms appear well described by single exponentials (lines). *B*, the rate of current activation increases with increasing hyperpolarization. Mean (±S.D.) activation time constants are plotted *vs.* voltage; each mean was derived from a minimum of twenty-four cells.

polarization (Fig. 1*B*). Subsequent experiments employing longer voltage steps and higher data acquisition rates, however, revealed clear deviations from this apparently simple exponential behaviour. Chief among these was the appearance of two distinct components of activation (Fig. 2). During 6 s hyperpolarizing voltage steps to potentials more negative than −80 mV, for example, the initial slow phase of inward current activation is followed by an even slower current increase (Fig. 2). Analyses of the inward current waveforms recorded during prolonged hyperpolarizations revealed that the data are poorly fitted by single exponentials (Fig. 2*A*), but are quite well fitted by the sum of two exponentials (Fig. 2*B*). The arrows in Fig. 2*A* indicate the regions of the curves that were judged (by eye) to be poorly fitted. When

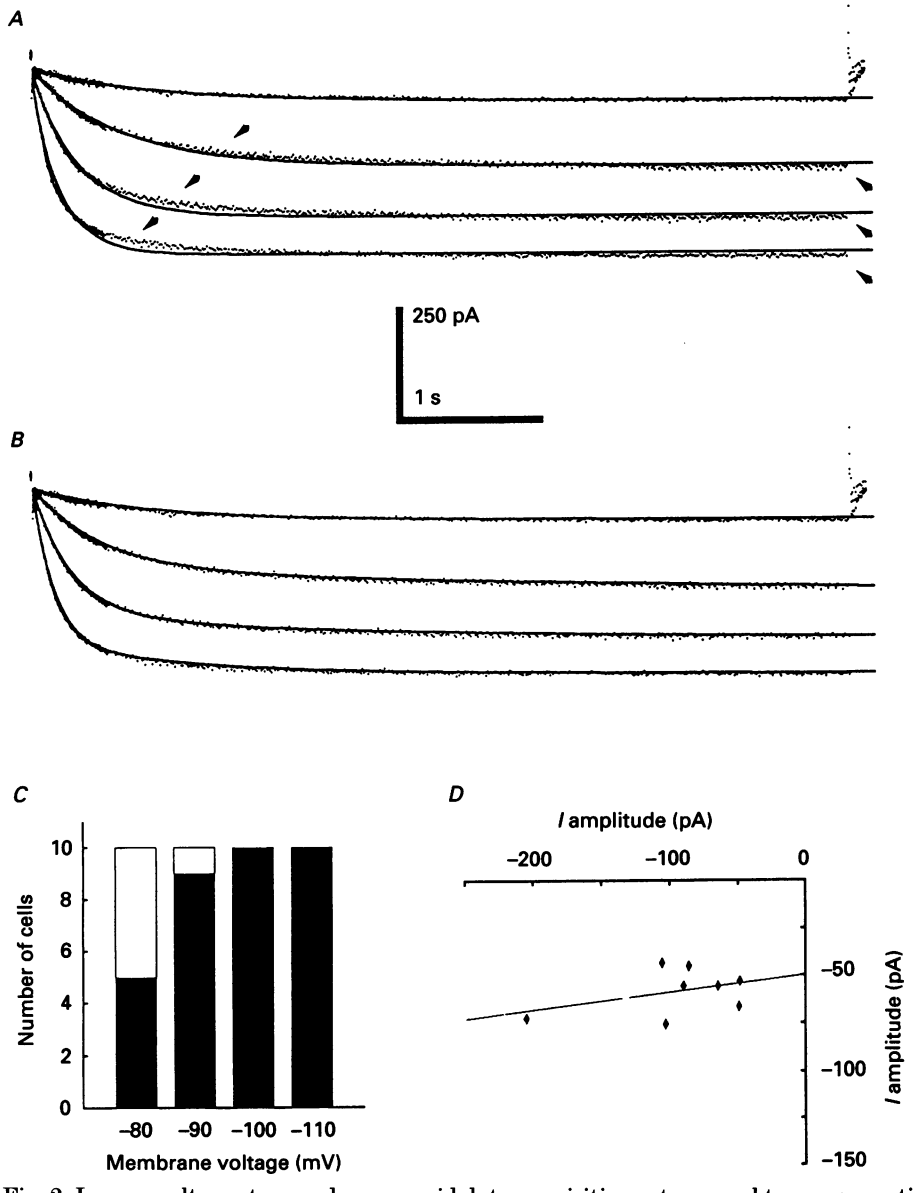

Fig. 2. Longer voltage steps and more rapid data acquisition rates reveal two exponential components of I_h activation. *A*, perforated patch recordings of inward currents (points) evoked during 6 s hyperpolarizing voltage steps to potentials between −80 and −110 mV from a holding potential of −40 mV. The current waveforms clearly deviate (arrowheads) from best-fitted (least squares) single exponential expressions (lines) at the more hyperpolarized potentials. *B*, currents evoked at test potentials negative to −80 mV are well described by the sum of two exponentials, corresponding to $I_{h,f}$ and $I_{h,s}$ (see text). *C*, in recordings similar to those illustrated in *A* and *B*, $I_{h,s}$ was observed in 10 of 10 cells examined at −100 and −110 mV, although it was more difficult to separate this current component at the more depolarized test potentials. Filled bars, number of cells with $I_{h,s}$; open bars, total number of cells studied. *D*, linear regression analysis of $I_{h,f,ss}$ *vs.* $I_{h,s,ss}$ (from eqn (2)) across cells; each point represents one cell. The slope of the best-fitted linear regression line (line) is not significantly different from zero.

the hyperpolarization-activated inward currents in SCP cells were examined during long voltage steps, the waveforms were routinely resolved into two distinct components. We have designated these $I_{h,f}$ and $I_{h,s}$, to denote the fast and slow components, respectively, of the total I_h activation.

In all subsequent experiments, therefore, activation was analysed by least squares fitting of the rising phases of the current waveforms using the following equation:

$$I = I_{inst} + I_{h,f,ss}(1 - e^{-(t-t_0)/\tau_{h,f}}) + I_{h,s,ss}(1 - e^{-(t-t_0)/\tau_{h,s}}), \quad (2)$$

where $I_{h,f,ss}$ is the steady-state amplitude of the faster component, $I_{h,s,ss}$ is the steady-state amplitude of the slower component, and $\tau_{h,f}$ and $\tau_{h,s}$ are the activation time constants of these respective components. $I_{h,f}$ activates with a voltage-dependent time constant of the order of hundreds of milliseconds while the slower exponential, $I_{h,s}$, activates with a time constant of the order of seconds. Although $I_{h,s}$ was consistently evident during voltage steps to the more hyperpolarized test potentials, it was less frequently distinguishable on steps to -80 mV or more positive potentials (Fig. 2*C*). This observation may, however, simply reflect the increased difficulty in resolving two exponentials at these more depolarized potentials due to low current amplitudes and very slow activation time courses. Because of the slow rates of activation of $I_{h,s}$, and its appearance during extreme hyperpolarizations, capacitative transient decays during hyperpolarizing voltage steps to -110 mV were fitted to eqn (1) to verify adequate spatial control of membrane voltage (see Methods). These analyses confirmed the presence of $I_{h,f}$ and $I_{h,s}$ in cells demonstrating adequate voltage control at -110 mV. The presence of two kinetically distinct I_h components could reflect two alternative or sequential gating pathways of *h*-channels or two functionally distinct populations of hyperpolarization-activated inward current channels. When the relative amplitudes of $I_{h,s,ss}$ and $I_{h,f,ss}$ in individual cells were compared (Fig. 2*D*), however, there was no correlation, suggesting that $I_{h,f}$ and $I_{h,s}$ do not reflect the sequential population of two open states of the same channel. Thus, $I_{h,f}$ and $I_{h,s}$ could reflect either two parallel gating pathways of the same channel or two distinct populations of channels. In either case, the data suggest that $I_{h,f}$ and $I_{h,s}$ are distinct and independent currents which, together, constitute the total time-dependent hyperpolarization-activated current in SCP neurons.

Activation delay

A second deviation from purely exponential current activation is apparent in Fig. 3*B*. Following hyperpolarizing voltage steps in the activation range of I_h, the subsequent time-dependent changes in inward current are not immediate, but rather are seen following a delay of many milliseconds.There is a finite plateau following the decay of the capacitance transient before the time-dependent increase in inward current is seen (Fig. 3*B*). At times soon after the onset of the hyperpolarizing voltage steps, the current waveforms in Fig. 3*B* are poorly fitted by eqn (2). In viewing the currents and the fits in Fig. 3*B*, however, it is clear that the presence of capacitative currents and the instantaneous, time-independent inward currents (i.e. all non-I_h currents) could complicate reliable analyses of the rising phases of I_h, particularly at times early after the onset of the hyperpolarizations. To better resolve the delay and

to clarify its source, therefore, currents were also recorded in the presence of caesium chloride. As previously reported (Solomon & Nerbonne, 1993), 3 mM caesium effectively blocks the time-dependent hyperpolarization-activated currents in SCP neurons leaving, primarily, I_{inst} (Fig. 3*C* and *D*). Digital off-line subtraction of the

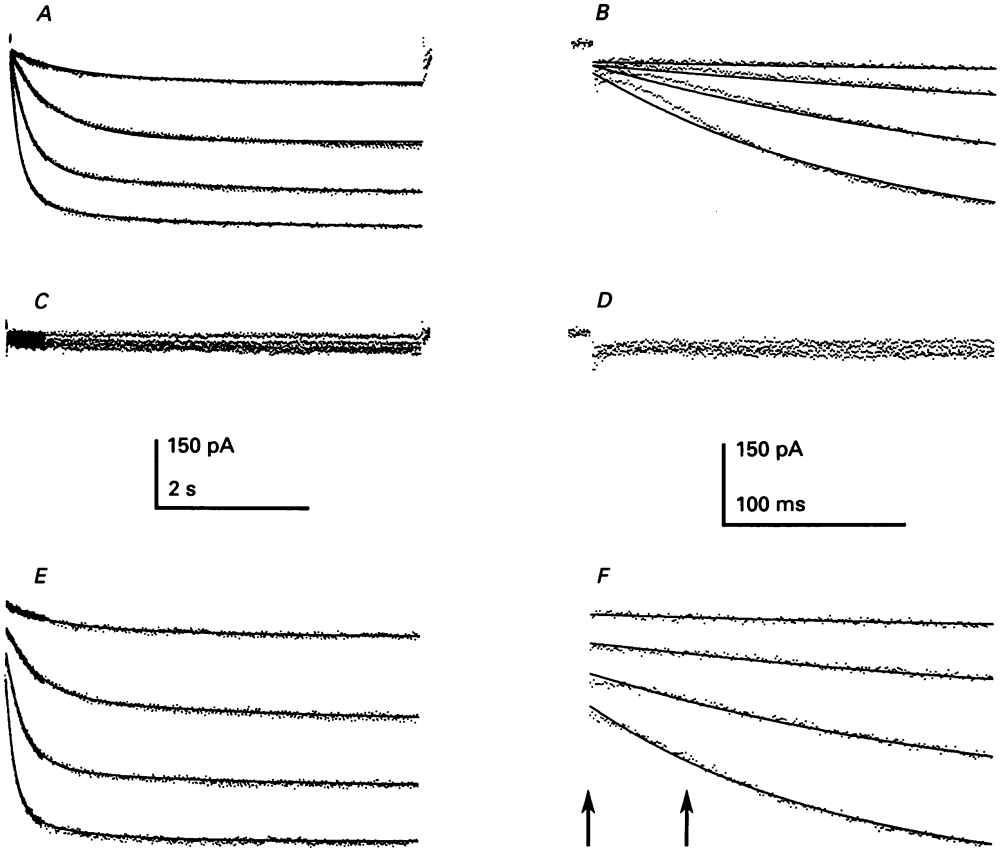

Fig. 3. Activation of $I_{h,f}$ is delayed. *A*, perforated patch recordings of inward currents (points) evoked during 6 s hyperpolarizations from −40 mV to test potentials between −80 and −110 mV appear to be well fitted by eqn (2) (lines). *B*, closer examination of the first 250 ms of current activation, however, reveals a delay in current activation following the decay of the capacitative transients, causing the data to be poorly fitted by a simple exponential at times soon after the onset of the hyperpolarizations. *C* and *D*, currents recorded during extracellular application of 3 mM CsCl to the same cell as in *A* and *B*. *E* and *F*, the caesium-sensitive currents were obtained by subtraction of the current records in *C* and *D* from those in *A* and *B*, respectively. Note that in *E* and *F* the traces have been offset from one another by −60 pA for the purpose of illustration. Also note that the activation delays remain in the subtracted records *F*, indicating that the delay does not result from either the capacitative currents or contaminating caesium-insensitive currents. The duration of the deviation from the fitted line is greatest for the trace recorded at −90 mV (the time course is indicated by the arrows) and becomes progressively shorter following more extreme hyperpolarizations.

currents recorded in the presence of caesium (Fig. 3*C* and *D*) from control current records (Fig. 3*A* and *B*, respectively) yields the caesium-sensitive inward currents (Fig. 3*E* and *F*, respectively). The subtraction procedure removes the residual

capacitative transients and eliminates I_{inst} (Fig. 3*E* and *F*), leaving only the time-dependent current waveforms. As illustrated in Fig. 3*F*, the activation delays (indicated by the arrows) remain in the subtracted records. In addition to revealing that both $I_{h,f}$ and $I_{h,s}$ are caesium-sensitive (Fig. 3*E*), these results suggest that the delay, because of its caesium sensitivity, is likely to be intrinsic to the activation of $I_{h,f}$. The low amplitude and very slow rate of activation of $I_{h,s}$, relative to that of $I_{h,f}$, make it impossible to determine if there is also a delay intrinsic to the gating of $I_{h,s}$.

To quantify these findings, the absolute magnitudes of the delays to the apparent start of h_f-current activation (apparent t_0) were determined explicitly by extrapolation of linearized current records back to the time at which $I_{h,f} = 0$. Because of the very slow activation of $I_{h,s}$, this current component was assumed not to contribute to the initial portions of the inward current waveforms and, for these analyses, was ignored. Rearranging eqn (2) for a single exponential and taking the natural logarithm of both sides yields:

$$\ln \frac{(I_{inst}+I_{h,f,ss})-I}{I_{h,f,ss}} = -\frac{1}{\tau_{h,f}}t+\frac{t_0}{\tau_{h,f}}, \quad (3)$$

where all symbols have their previously defined meanings. For times after the initial delay, single exponential current activation data plotted in this manner fall on a straight line with slope of $-1/\tau_{h,f}$ and a y-intercept of $t_0/\tau_{h,f}$ (Fig. 4*A* and *B*). The onset of I_h activation was determined by least squares fitting of the initial linear portion of the inward current waveforms and subsequent extrapolation of the regression lines to the x-axis to determine apparent t_0 values. Activation delays, as defined by the difference between these analytically determined values for t_0 and the actual time of initiation of the hyperpolarizing voltage steps, are plotted as a function of voltage in Fig. 4*C* and *D*. The delay in current activation for the raw current traces is voltage dependent ($P < 0{\cdot}05$ by MANOVA), decreasing at more hyperpolarized potentials. Similar analyses of the caesium-sensitive current records (Fig. 4*D*) also revealed the presence of apparent delays prior to the activation of I_h that were not significantly different (paired t tests) from those determined from the raw current records (Fig. 4*C*).

Following the subtraction of caesium-insensitive currents, it is clear that the activation delay imparts an S-shape to the waveforms of hyperpolarization-activated currents (see Fig. 3*F*). Sigmoidal activation is reminiscent of several other types of voltage-activated conductances in which channel opening is thought to require prior transitions through multiple closed states (Hodgkin & Huxley, 1952; Bezanilla, 1985). I_h activation, therefore, was modelled as the product of a Hodgkin–Huxley type multi-state reaction sequence (Hodgkin & Huxley, 1952) according to eqn (4):

$$I = I_{inst}+I_{h,f,ss}(1-\exp(-(t-t_0)/\tau_{h,f}))^{n_{h,f}}+I_{h,s,ss}(1-\exp(-(t-t_0)/\tau_{h,f}))^{n_{h,s}}, \quad (4)$$

in which $n_{h,f}$ and $n_{h,s}$ reflect the number of closed state transitions (or subunits) participating in h_f- and h_s-channel gating, respectively, and all other symbols have their previously defined meanings. Again, $I_{h,s}$, because of its very slow kinetics of activation, was assumed not to contribute substantially to the initial portion of the time-dependent inward current and was assigned purely exponential activation (i.e.

$n_{h,s} = 1$). The sigmoidal activation of $I_{h,f}$ in Fig. 3*F* is clearly not accounted for by a model with $n_{h,f} = 1$, conditions under which eqn (4) reduces to eqn (2). Nevertheless, attempts to fit the data with exponents greater than or equal to two also resulted in poor fits to the data (not shown). Subtracted current records were,

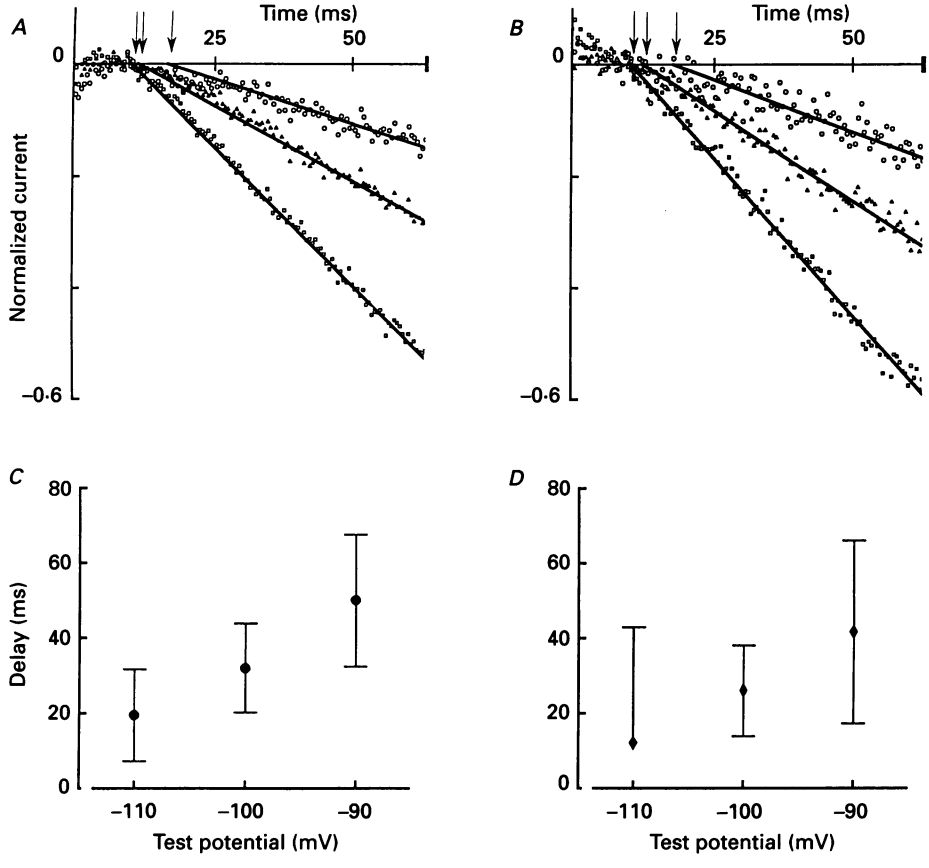

Fig. 4. $I_{h,f}$ activation delay is voltage dependent. To quantify the delay, currents recorded during steps between −90 and −110 mV were transformed according to eqn (3) and then fitted by least squares linear regression over the initial linear portion of current activation. The data points (○ = −90 mV, ▲ = −100 mV, □ = −110 mV) and the fitted lines for both the raw (*A*) and the caesium-subtracted (*B*) current records are shown. The apparent t_0 at each potential, determined by extrapolation of the linear regression line to the time axis, is indicated by an arrow. Activation delays, calculated as the difference between the apparent t_0 and the actual initiation of the voltage step, are plotted as a function of step potential for the raw (*C*) and the caesium-subtracted (*D*) current records. The delays in both *C* and *D* are significantly longer (MANOVA) at more depolarized potentials. Moreover, the values obtained from the raw current records are not significantly different (paired *t* tests) from those obtained from analyses of the caesium-sensitive currents.

therefore, refitted to eqn (4) using non-linear least squares regression in which $n_{h,f}$ was a free parameter whose value was permitted to be non-integral. As shown in Fig. 5*A* and *B*, the solutions to eqn (4) (for the same records as those presented in

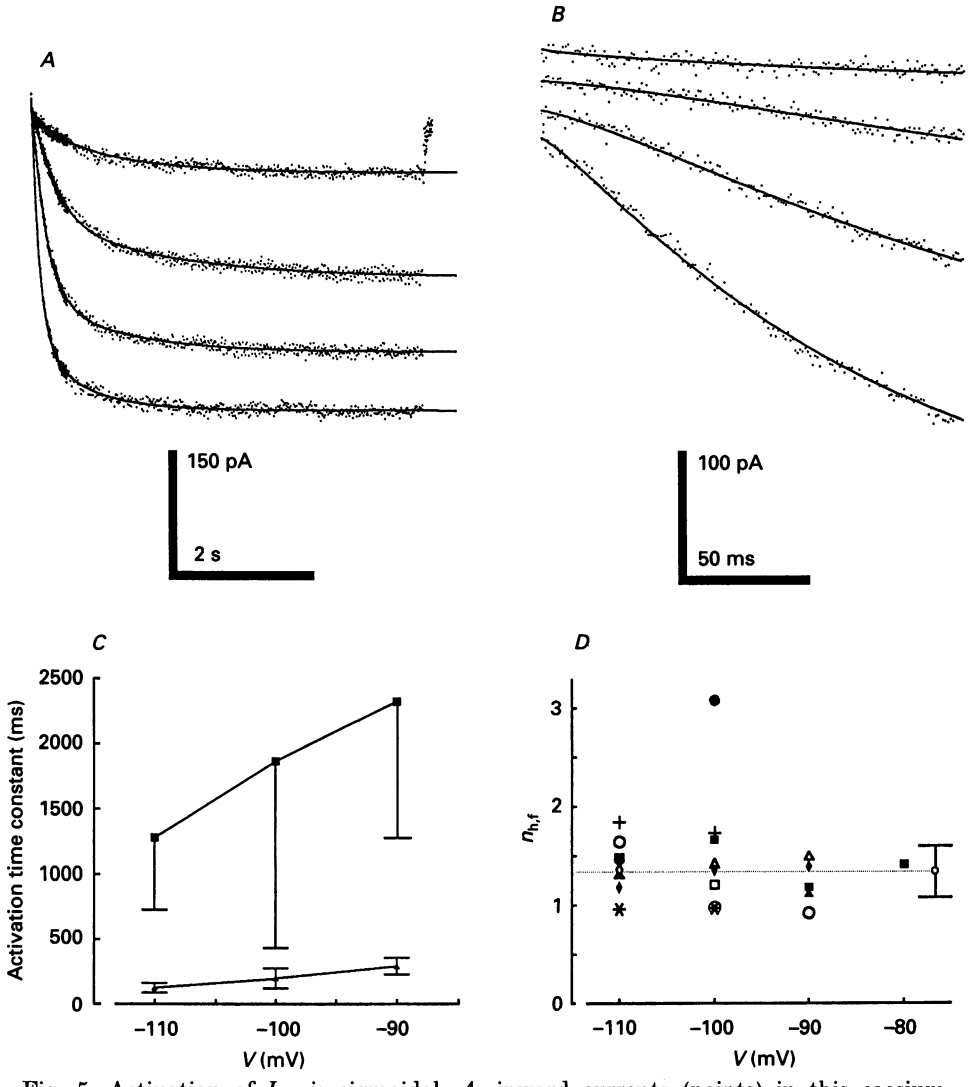

Fig. 5. Activation of $I_{h,f}$ is sigmoidal. *A*, inward currents (points) in this caesium-subtracted perforated patch recording are plotted with the best least squares fits to eqn (4). *B*, expanded traces of the records shown in *A* demonstrate that the sigmoidal nature of current activation is well accounted for by a value of $n_{h,f}$ near 1·3. Note that the current records have been offset from one another by −20 pA for illustration. *C*, mean (±S.D.) time constants for $I_{h,f}$ (▲) and $I_{h,s}$ (■) activation, derived from fits to eqn (4) plotted *vs.* test potential. The rate of activation is voltage-dependent for both current components and, at all test potentials, the time constants of activation for $I_{h,f}$ and $I_{h,s}$ differ by approximately an order of magnitude. *D*, from eqn (4), the exponent for $I_{h,f}$ activation, $n_{h,f}$, is plotted as a function of test potential. Each symbol represents the data from one cell. The mean (±S.D.) value for $n_{h,f}$ (1·34) is shown at the far right. The outlying point at −100 mV (●) was not included in the calculation of the mean.

Fig. 3*E* and *F*) provided excellent fits to the data ($r \geqslant 0{\cdot}990$). Nevertheless, the lower signal to noise ratio associated with the small amplitude currents evoked during steps to −80 mV or more depolarized potentials made parameter estimates less reliable at these potentials. Mean (±S.D.) values for $n_{h,f}$ were $1{\cdot}4 \pm 0{\cdot}3$ at −110 mV

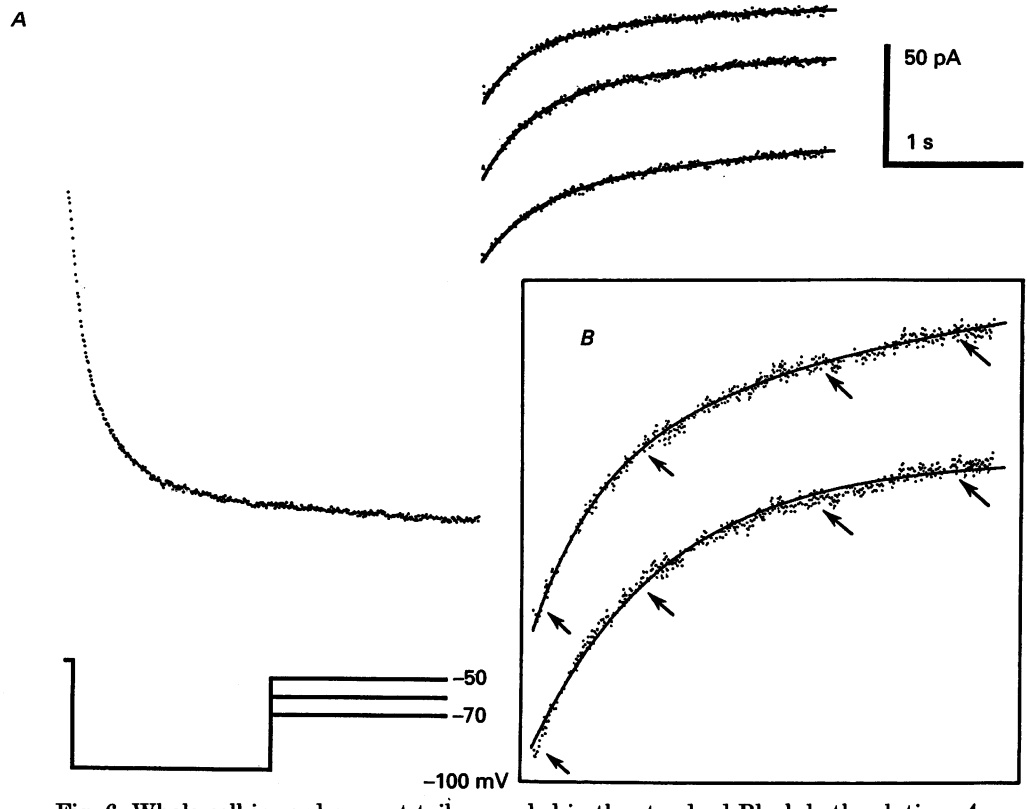

Fig. 6. Whole-cell inward current tails recorded in the standard Block bath solution. *A*, tail currents were recorded at potentials between −70 and −50 mV following a 3 s hyperpolarization to −100 mV; the protocol is illustrated below the current traces. For clarity, the current recorded at −100 mV is displayed only for one sequence (for the −70 mV tail). The records shown are unsubtracted, although subtraction protocols (see text) were used for determination of all deactivation time constants for tail currents recorded during steps to −60 mV or more depolarized potentials. At all potentials, the current tails (points) were well described by least squares regression fits (lines) to the sum of two exponentials (eqn (5)). *B*, for comparison of the quality of the fits, the tail current (points) recorded at −70 mV is reproduced twice and shown fitted (continuous lines) with the sum of two exponentials (upper trace) and with a single exponential (lower trace). Portions of the current trace clearly deviate from the single exponential fit (arrows, lower trace), unlike the corresponding positions marked by arrows in the double exponential fit (upper trace).

($n = 8$) and $1{\cdot}2 \pm 0{\cdot}2$ at −90 mV ($n = 5$), with no significant voltage dependence (repeated measures MANOVA). The overall mean (±S.D.) for $n_{h,f}$ at all test potentials was $1{\cdot}34 \pm 0{\cdot}26$ ($n = 22$). A non-integral value for n, however, is not readily

interpretable in terms of the number of *identical* and *independent* channel closed state transitions participating in the activation process, and suggests the participation of two or more energetically *non-equivalent* closed state transitions in the process of h_f-channel opening (see Discussion).

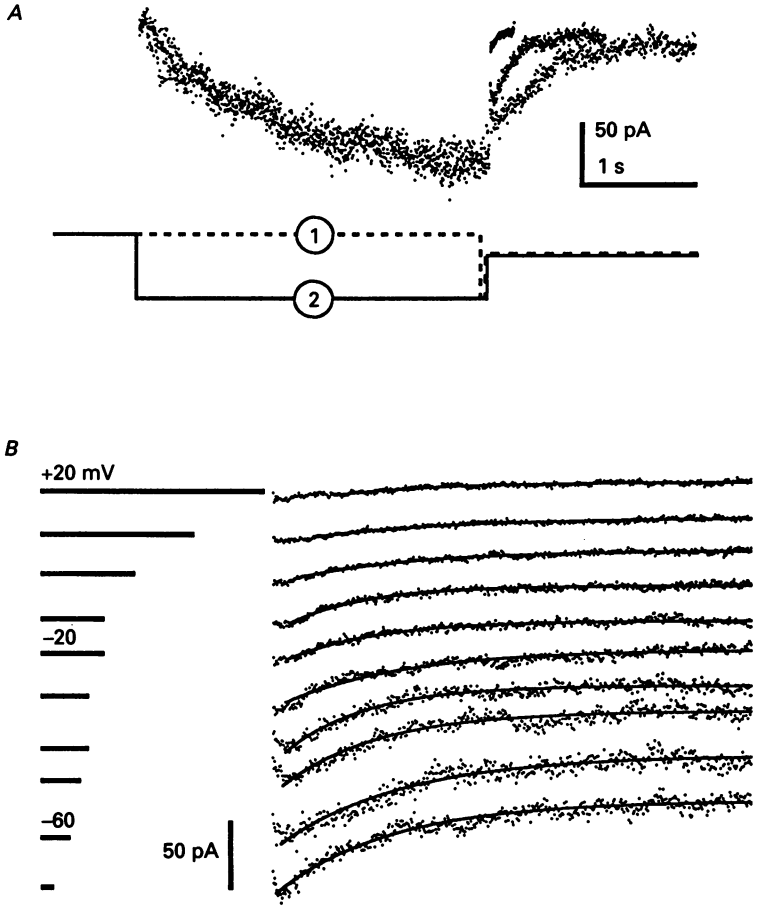

Fig. 7. Tail currents recorded in 120 mM KCl bath with 140 mM CsCl pipette solution. *A*, representative subtracted and averaged whole-cell activation records and current tails recorded on repolarization to −60, −40 and +20 mV. As shown in the protocol, current tails recorded following brief hyperpolarizing voltage steps to −100 mV (1) were subtracted from current tails recorded following 3 s step to −100 mV (2). Because of the ionic composition of the recording solutions, tail currents at all test voltages were inward. *B*, subtracted and averaged tail currents (points) and least squares best-fitting single exponential decays (lines) are shown for repolarizations between −70 (bottom trace) and +20 mV (top trace). Except for the tail current recorded during repolarization to −70 mV, none of the tail currents were substantially better fitted by a double exponential decay (eqn (5)) than by the single exponential decay shown. The horizontal scale bar next to each trace indicates 100 ms.

Deactivation of the hyperpolarization-activated inward currents

Deactivation of the hyperpolarization-activated inward currents in SCP neurons also appeared to follow a time course described by the sum of two exponentials. The kinetics of current deactivation were examined by recording tail currents during test

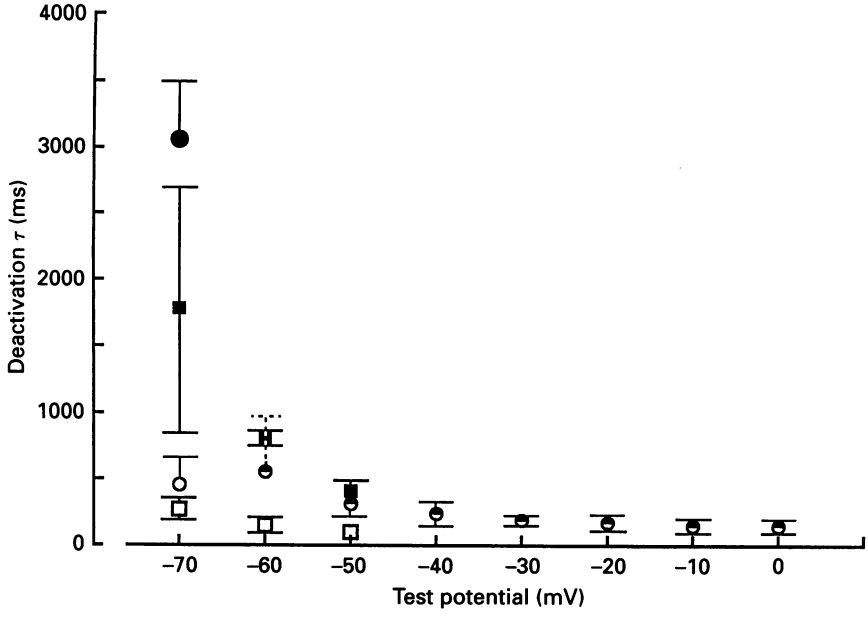

Fig. 8. Time constants of deactivation. The mean (±S.D.) time constants determined from tail current decays, recorded in standard Block bath solution (as in Fig. 6) or in 120 mM KCl bath solution (as in Fig. 7) are plotted *vs.* test potential. Tail current decays in Block bath solution are well described by the sum of two exponentials. The time constants of the fast (□) and slow (■) exponential components decreased with increasing depolarization. Deactivations recorded with 140 mM CsCl pipette solution in 120 mM KCl bath solution, were biexponential only at −70 mV. The mean deactivation time constants for the fast (○) and slow (●) components at this potential were larger than the corresponding time constants measured in Block bath solution, although this difference was not significant (*t* test). At potentials more depolarized than −70 mV, tail current decays recorded in 120 mM KCl bath were well described by single exponentials with mean (±S.D.) time constants (○) at −60 and −50 mV intermediate in magnitude between the two time constants resolved in Block bath solution.

voltage steps to potentials between −70 and −50 mV following 3 s hyperpolarizations to −100 mV to activate $I_{h,f}$ and $I_{h,s}$ (Fig. 6). To examine the kinetics of tail current decay, an alternative voltage clamp protocol was developed in which the contaminating current tails were subtracted from the total tail currents to isolate $I_{h,f}$ and $I_{h,s}$ tails. The protocol, illustrated in Fig. 7, consisted of two steps: tails were first recorded following a 20 ms pulse to −100 mV, a period too brief to permit substantial activation of $I_{h,f}$ and $I_{h,s}$, and subsequently following a 3 s hyperpolarization to −100 mV. The currents recorded during the first sequence were then subtracted from those recorded during the second, and the resulting subtracted

records were then averaged over two to five trials. Although attempts were made to fit the averaged, subtracted records to eqn (4), the noise associated with these low amplitude current records precluded determining whether n was $\geqslant 1$. Current tails were fitted instead to the following expression, which is similar to eqn (2):

$$I = I_{\text{inst}} + I_{\text{fast, peak}}(\exp(-t-t_0)/\tau_{\text{fast}}) + I_{\text{slow, peak}}(\exp(-t-t_0)/\tau_{\text{slow}}), \quad (5)$$

TABLE 1. Recording Solutions*† (mM)

	$[Na^+]$	$[K^+]$	$[Cl^-]$	$[Mg^{2+}]$	$[Ca^{2+}]$	[EGTA]	$[SO_4^{2-}]$	$[Cs^+]$	$[Co^{2+}]$
Pipette‡									
K^+–Ca^{2+} buffer	1·5	140	—	3	2·07	10	—	—	—
Nystatin§	—	195	69	7	—	—	70	—	—
140 caesium	4	—	—	3	2·07	10	—	140	—
Bath‖									
Block	120	4	149	2	0·5	—	—	—	2
120 KCl	4	120	153	2	0·5	—	—	—	2

* All solutions contained 10 mM Hepes adjusted to pH 7·3 with KOH, NaOH, or Tris base.
† All solutions contained 5 mM glucose.
‡ All whole-cell pipette solutions contained 3 mM ATP and 0·5 mM GTP.
§ Nystatin pipette solution contained 0·1 mg/ml nystatin and 0·2% dimethyl sulphoxide.
‖ Bath solutions contained 1 μM TTX, 20 mM TEA, and 1 mM 4-aminopyridine except as noted in the text.

where $I_{\text{fast, peak}}$ and $I_{\text{slow, peak}}$ are the peak amplitudes of the rapidly and the slowly deactivating components respectively, τ_{fast} and τ_{slow} are the deactivation time constants of the respective components, t_0 is the time at the beginning of the deactivating voltage pulse, and all other symbols have their previously defined meanings. As illustrated in Fig. 6*A*, the tail current decays are well described by eqn (5), but poorly fitted by a single exponential (Fig. 6*B*). Time constants decreased with increasing depolarization: the mean (±S.D.) τ_{fast} ranged from 355+161 ms at −70 mV (n = 7) to 99±8 ms at −50 mV (n = 3) and the mean (±S.D.) τ_{slow} ranged from 2428±1285 ms at −70 mV ($n = 6$) to 413±78 ms at −50 mV ($n = 3$). These values are plotted in Fig. 8.

To examine $I_{h,f}$ and $I_{h,s}$ deactivation at more depolarized potentials without contamination by voltage-activated outward potassium currents, additional experiments were performed using a pipette solution in which 140 mM caesium chloride replaced the usual KCl (Table 1). Unlike extracellular caesium (Fig. 3*C* and *D*), intracellular caesium does not block time-dependent hyperpolarization-activated inward currents. In addition, extracellular potassium was increased to 120 mM in these experiments to increase the conductance (Solomon & Nerbonne, 1993), thereby permitting better resolution of the tail currents. Under these ionic conditions, hyperpolarization-activated current tails were inward at all test potentials. The paired subtraction protocol used to isolate the tail currents was identical to that described above (Fig. 7). As in the previous experiments, inward current tails at −70 mV were biexponential (Fig. 7*B*) with fast and slow time constants that were not significantly different (*t* test) from those recorded using the 140 mM KCl pipette solution (Fig. 8). At test potentials more depolarized than −70 mV, however, tail current decays were well described by single exponentials (Fig. 7*B*). At test

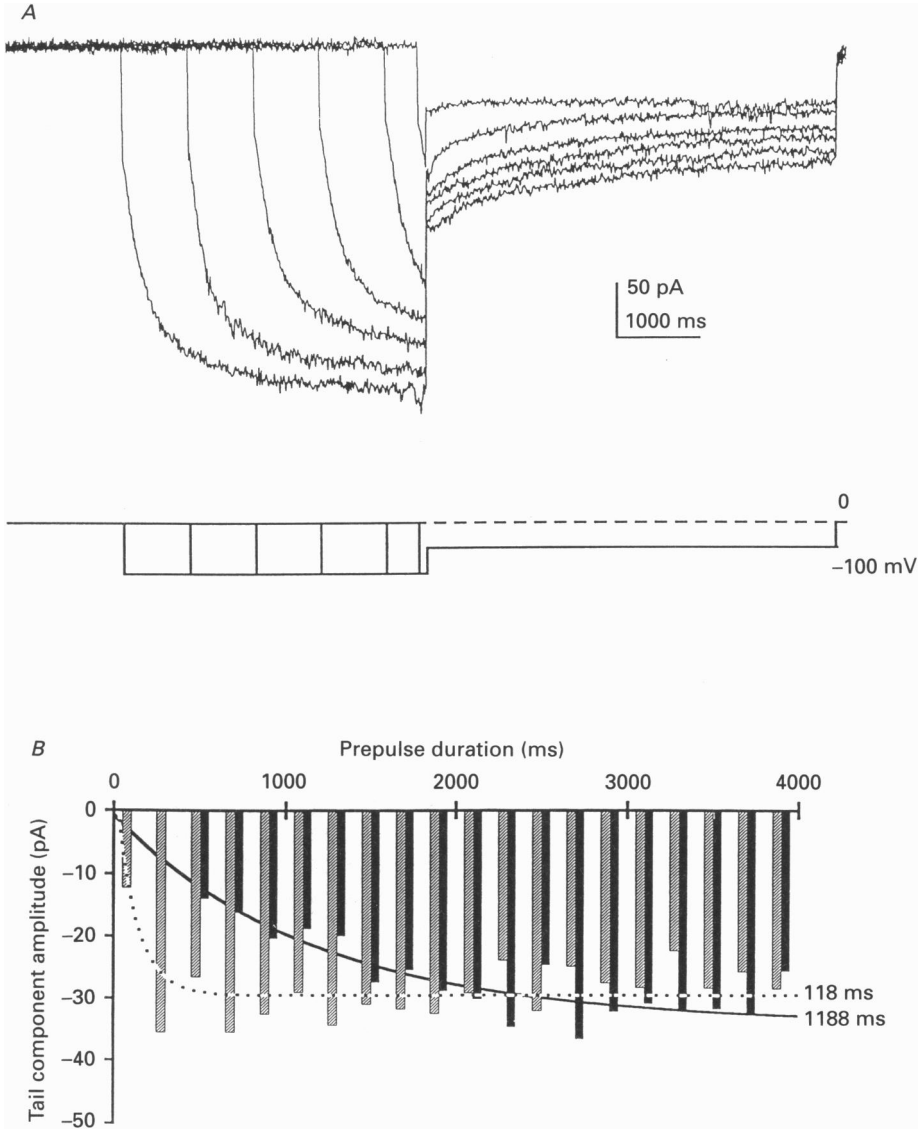

Fig. 9. The rapidly and slowly deactivating tail current components correspond to $I_{h,f}$ and $I_{h,s}$, respectively. *A*, whole-cell recordings of tail currents at −70 mV reveal an increase in amplitude following repeated, progressively longer prepulses to −100 mV. Only selected traces are shown for clarity. *B*, peak amplitudes of the two components were determined from biexponential fits to the tail current decays for the experiment shown in *A*, and are plotted here as a function of prepulse duration. The rapid increase and plateau of the more rapidly deactivating tail current component (hatched bars) parallels the activation of $I_{h,f}$. The subsequent gradual increase in the slowly deactivating tail current component (filled bars) parallels the time course of activation of $I_{h,s}$. Also shown are single exponential least squares fits (eqn (6)) to the tail current envelopes of the rapidly deactivating tail current component (dotted line) and the slowly deactivating tail current component (filled line). These time constants are virtually identical to the current activation time constants for $I_{h,f}$ and $I_{h,s}$ measured directly in this cell at −100 mV (see text).

potentials of −60 mV and −50 mV, where tail current decays could be compared under the two recording conditions, the single time constant recorded with 140 mM Cs^+ was intermediate in magnitude between the two time constants obtained with 140 mM K^+ (Fig. 8).

The similarity in the amplitudes of the activation and deactivation time constants near the half-activation voltage for the total hyperpolarization-activated current (Solomon & Nerbonne, 1993) suggests that the faster tail current decay reflects the deactivation of $I_{h,f}$ and that the slower tail current decay reflects the deactivation of $I_{h,s}$. To test this hypothesis, the envelope of fast and slow tail current components was examined following step increases in the degree of activation of $I_{h,f}$ and $I_{h,s}$. As shown in Fig. 9*A*, cells were repeatedly hyperpolarized to −100 mV for gradually increasing lengths of time and the tail currents were recorded on return of the membrane voltage to −70 mV. The peak amplitude of each tail component was then determined using eqn (5) in which τ_{fast} and τ_{slow} were set equal to their mean values at −70 mV (Fig. 9). Examination of the tail component amplitudes consistently ($n = 3$) revealed that $I_{fast,peak}$ rapidly increased in amplitude to a steady state following 300 ms hyperpolarizations, whereas $I_{slow,peak}$ increased much more slowly, and achieved its steady-state amplitude only after several seconds. Example tail component envelopes for one such cell are shown in Fig. 9*B* along with least squares best-fitted lines to the single exponential expression:

$$I_{tail} = I_{peak}(1-\exp(-t_{act}/\tau)), \tag{6}$$

where I_{peak} is the tail component peak amplitude, t_{act} is the duration of the voltage step to −100 mV, and τ is the time constant of the fitted line. The time constants of the fast tail component envelope (118 ms) and the slow tail component envelope (1188 ms) are virtually identical to the values for $\tau_{h,f}$ and $\tau_{h,s}$ measured in this cell directly using eqn (2) (224 and 1193 ms, respectively), consistent with the interpretation that τ_{fast} reflects the deactivation of $I_{h,f}$, and τ_{slow} reflects the deactivation of $I_{h,s}$.

Inactivation of hyperpolarization-activated inward currents

Inactivation from the open state was investigated by examining current waveforms during long hyperpolarizing pulses. As shown in Figs 2, 3, and 5, current decrements were never observed at any test potential during 6 s hyperpolarizing voltage steps. Moreover, the hyperpolarization-activated inward currents in these cells do not decrease over time during step hyperpolarizations lasting as long as 18 s (not shown).

Closed state inactivation was examined by holding the cell at potentials depolarized with respect to the activation threshold for the total hyperpolarization-activated current (Solomon & Nerbonne, 1993) and then testing the activatable time-dependent inward current. As shown in Fig. 10, inward current traces at −100 mV following 10 s prepulses between −40 and 0 mV superimpose. Therefore, hyperpolarization-activated inward current channels available for opening from a holding potential of −40 mV remained available for opening following depolarization to 0 mV. Taken together, these results suggest that the time-dependent inward currents, $I_{h,f}$ and $I_{h,s}$ display neither open state nor closed state inactivation.

DISCUSSION

Two components of I_h in SCP neurons

The time-dependent hyperpolarization-activated inward currents in SCP neurons are distinguished from many other well-characterized voltage-activated conductance

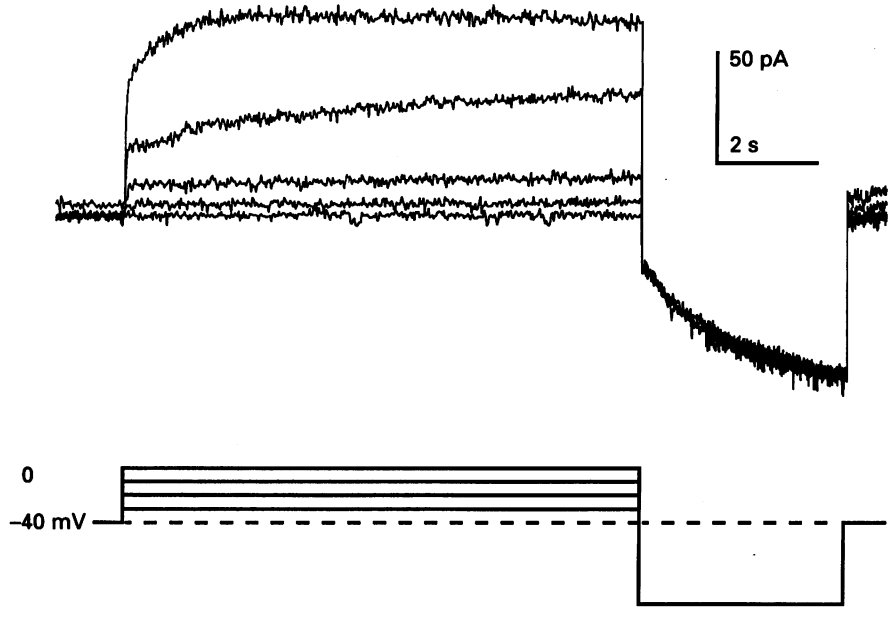

Fig. 10. $I_{h,f}$ and $I_{h,s}$ do not exhibit closed state inactivation. Whole-cell hyperpolarization-activated inward currents were recorded following 10 s prepulses to potentials between −40 and 0 mV. Note that depolarizations prior to channel activation do not alter the current waveforms.

pathways in these (Giffin *et al.* 1991) and other neuronal cells (see Llinas, 1988) by their extraordinarily slow rates of activation and deactivation. Slow kinetics are, however, shared by a collection of non-traditional inward rectifier currents that have been described in other systems, including I_f in sino-atrial node (Van Ginneken & Giles, 1991) and Purkinje fibres (Hart, 1983; DiFrancesco, 1984), I_Q in lobster stretch receptors (Edman, Gestrelius & Grampp, 1987), and *h*-currents in a variety of other neuronal preparations (Attwell & Wilson, 1980; Attwell, Werblin & Wilson, 1982; Mayer & Westbrook, 1983; Hestrin, 1987; McCormick & Pape, 1990). In Purkinje fibres (DiFrancesco, 1984), for example, I_f activates with complex kinetics but generally over a time course of hundreds of milliseconds to a few seconds at 35 °C. I_f (DiFrancesco, 1984), I_Q (Edman *et al.* 1987) and I_h (Mayer & Westbrook, 1983; Hestrin, 1987) also share in common relatively depolarized reversal potentials, permeability to sodium and potassium and sensitivity to millimolar concentrations of extracellular Cs^+.

Unlike most previous descriptions of hyperpolarization-activated inward currents, however, the analyses here reveal that I_h in SCP neurons is composed of two kinetically distinct components, that we have designated $I_{h,f}$ and $I_{h,s}$. Although both

components display properties similar to other non-traditional inward rectifier currents in other preparations, they are separable based on their differing kinetics of activation and deactivation. At −90 mV, for example, the mean (±S.D.) activation time constant of $I_{h,f}$ is 292±66 ms ($n = 5$); whereas, the mean (±S.D.) activation time constant for $I_{h,s}$ is 2324±1043 ms ($n = 5$). These distinct components of I_h activation may be similar to the fast and slow components of the hyperpolarization-activated inward current described in layer V neurons from cat sensorimotor cortex (Spain, Schwindt & Crill, 1987). $I_{h,f}$ and $I_{h,s}$ deactivation time constants at −70 mV were also readily distinguishable with mean (±S.D.) values of 355±161 ms ($n = 7$) and 2428±1285 ms ($n = 6$), respectively. Reliable time constant estimates for $I_{h,f}$ and $I_{h,s}$ activation and deactivation between these two voltages, presumably in the region of half-activation (Solomon & Nerbonne, 1993), were difficult to determine, primarily due to the low-current amplitudes.

Use of 140 mM intracellular caesium chloride and 120 mM extracellular potassium chloride permitted the measurement of tail currents over a much wider voltage range without contamination by voltage-activated outward potassium currents. Separate $I_{h,f}$ and $I_{h,s}$ tail components could not, however, be resolved except during the largest of these relaxations recorded at −70 mV. The tail currents recorded under these conditions were well-fitted by single exponentials whose time constants probably represent some combination of the individual decay time constants of $I_{h,f}$ and $I_{h,s}$.

In Fig. 9, the deactivation time constants for $I_{h,f}$ and $I_{h,s}$ may be slowed by the change of the ionic composition of the recording solutions. Increased extracellular potassium reportedly increases the time constant of deactivation of I_f in sheep Purkinje fibres (Hart, 1983). Slowing the open → closed transition rates of $I_{h,f}$ and $I_{h,s}$ channels could explain, at least in part, the mechanism by which increases in extracellular potassium can increase the total I_h conductance in these cells (Solomon & Nerbonne, 1993).

It is unclear whether $I_{h,f}$ and/or $I_{h,s}$ share molecular similarity with the I_h, I_f, or I_Q conductance pathways described in other systems. The time constants determined in our experiments at room temperature are not directly comparable to those determined in other preparations at 35 °C without information on how the rates of current activation and deactivation change with temperature. Nevertheless, using an estimated Q_{10} of 3 (Hart, 1983; Angstadt & Calabrese, 1989), the reported time constants for inward current activation adjusted for measurements at 37 °C are largely comparable in cat and guinea-pig thalamus (McCormick & Pape, 1990), rabbit sino-atrial node (Van Ginneken & Giles, 1991), sheep Purkinje fibres (Hart, 1983), and leech heart interneurones (Angstadt & Calabrese, 1989), being approximately 400 ms at −90 mV. This time constant might be expected for the activation of $I_{h,s}$ at 37 °C. The activation time constants for $I_{h,s}$, however, overlap with the activation time constants measured for the total time-dependent inward current in SCP neurons. It remains possible, therefore, that the hyperpolarization-activated inward currents in other systems may also be resolvable into multiple distinct components.

Although not previously investigated in detail, the existence of a second hyperpolarization-activated current component has been reported in heart (DiFrancesco, 1984), dorsal root ganglion neurons (Mayer & Westbrook, 1983), and

thalamic relay neurons (McCormick & Pape, 1990; compare their Fig. 3*D* with our Fig. 2). Clarification of the numbers of hyperpolarization-activated current components and their properties will become particularly important in determining their roles in modulating cellular electrical activity.

Gating of I_h channels in SCP neurons

On membrane hyperpolarization, activation of time-dependent inward currents in SCP neurons proceeds following a voltage-dependent delay, similar to hyperpolarization-activated currents in other systems (DiFrancesco & Ferroni, 1983; Hart, 1983; DiFrancesco, 1984; Edman *et al.* 1987; Hestrin, 1987; Angstadt & Calabrese, 1989; Van Ginneken & Giles, 1990). The delay was approximately 50 ms at −90 mV, but was nearly undetectable at −110 mV. As is the case for I_f in Purkinje fibres (DiFrancesco, 1984), the delay was not significantly changed by off-line subtraction of the caesium-insensitive currents, suggesting that the delay is caesium-sensitive and intrinsic to current activation. Because $I_{h,s}$ activation is so slow, it is unlikely that a delay intrinsic to this component would be detectable in the presence of $I_{h,f}$. In support of this hypothesis, the rising phases of the currents were well fitted by eqn (2) in which the delay was considered to be intrinsic to $I_{h,f}$ activation, and $I_{h,s}$ is proposed to activate with purely single exponential kinetics.

Previous descriptions of inward current activation in other systems have advanced a variety of theories to account for the delay. In studies of I_f in rabbit sino-atrial node cells, for example, Van Ginneken & Giles (1991) employed a traditional Hodgkin–Huxley model with $n = 2$, although they did note that a more complicated scheme may be required to account for some aspects of inward current activation. In contrast, studies of I_f in calf Purkinje fibres (DiFrancesco, 1984) suggest that the Hodgkin–Huxley power function exponent varies between the values of one and three in a voltage-dependent manner, leading DiFrancesco (1984) to propose a complex model describing voltage-dependent transitions between five open states and three closed states. Other models include the combination of two single exponential functions of opposite sign (Hestrin, 1987), and a three-state model involving both voltage-dependent and voltage-independent transitions (Edman *et al.* 1987).

The data in Fig. 5 demonstrate that the sigmoidal activation of $I_{h,f}$ in SCP neurons is well fitted by a power function; however, the value of the exponent, $n_{h,f}$, is non-integral. The sigmoidal nature of the activation indicates a requirement for $n_{h,f}$ to be greater than one. Because attempts to fit the data with $n_{h,f}$ set equal to two did not improve the quality of the fits, however, $n_{h,f}$ was allowed to vary among all real numbers as a free parameter. This strategy has previously been used to describe the sigmoidal activation of the sodium current in squid axon (Keynes, Kimura & Greeff, 1988). As shown in Fig. 5*D*, the model was best fitted to the data with $n_{h,f}$ (mean ± S.D.) equal to 1·34 ± 0·26 at all test potentials. The mechanistic interpretation of a non-integral value for $n_{h,f}$, however, is problematic in terms of the traditional Hodgkin–Huxley formalism (Hodgkin & Huxley, 1952). Nevertheless, the lack of variation of $n_{h,f}$ with test potential is consistent with the idea that $n_{h,f}$ describes, in some fashion, the number of subunits or closed states participating in the gating of hyperpolarization-activated inward currents in SCP neurons. Because the Hodgkin–Huxley formalism is based on a reaction sequence involving multiple

independent and identical gating particles, we interpret the non-integral value for $n_{h,f}$ to reflect non-identity of the gating subunits and/or non-independence (co-operativity) in the gating reaction. A value for $n_{h,f}$ of 1·3 thus suggests that a minimum of two conformational changes are involved in the opening of $I_{h,f}$ channels and that these conformational changes are energetically non-equivalent due to dissimilarity of the protein domains participating in channel gating and/or the alteration of the rate of one transition by a previous transition. Current kinetics that are incompatible with a gating reaction involving multiple identical (independent) transitions have also been reported for the sodium current and the delayed rectifier potassium current in squid giant axon (Bezanilla, 1985) and, more recently, for cloned voltage-gated K^+ channels expressed in *Xenopus* oocytes (Tytgat & Hess, 1992).

It is unclear from our data whether deactivation of the hyperpolarization-activated inward currents is sigmoidal as well. Attempts to determine the value for n during current deactivation by fitting current tails to an expression similar to eqn (4) gave inconsistent results. The variability in these measurements probably derives from the noise associated with these low amplitude currents, as well as the occasional appearance of rapid current relaxations at the beginning of subtracted current records using 140 mM CsCl pipette solution and 120 mM KCl bath solution. Sigmoidal deactivation has been observed in both cardiac (DiFrancesco, 1984; Van Ginneken & Giles, 1991) and neuronal (Edman *et al.* 1987; Hestrin, 1987) preparations.

Physiological roles of $I_{h,f}$ and $I_{h,s}$

The very slow kinetics and lack of inactivation of the hyperpolarization-activated inward currents in SCP neurons suggest that these currents will influence the resting membrane potential, as well as the pattern of action potential firing over tens to hundreds of milliseconds. In a quiescent SCP neuron with an average resting membrane potential of −66 mV, hyperpolarization-activated inward currents are appreciably activated (Solomon & Nerbonne, 1993). As a result, $I_{h,f}$ and $I_{h,s}$ are expected to influence responses to depolarizing and hyperpolarizing inputs both directly, by influencing resting input resistance, and indirectly, by modulating the resting membrane potential and, consequently, voltage-dependent membrane processes.

In addition, the slow activation and deactivation kinetics of $I_{h,f}$ and $I_{h,s}$ are expected to lead to novel time-dependent influences on SCP neuron electrical activity. Unlike most voltage-activated currents described in cortical neurons, activation and deactivation of both $I_{h,f}$ and $I_{h,s}$ are probably too slow to contribute to the waveforms of individual action potentials. In contrast, these currents are expected to contribute to shaping patterns of cellular electrical activity over tens to hundreds of milliseconds. During a maintained hyperpolarization, such as during $GABA_B$ receptor-mediated IPSPs (Newberry & Nicoll, 1985; Connors, Malenka & Silva, 1988), for example, the activation of $I_{h,f}$ and $I_{h,s}$ would act as a slow negative feedback regulator of membrane potential. Due to the depolarized reversal potential of I_h (Solomon & Nerbonne, 1993), the effect of current activation on a maintained hyperpolarization is a depolarizing *sag* toward the resting membrane potential. Perhaps more importantly, the slow time course of current deactivation will, on removal of the hyperpolarizing input, cause a transient *overshoot* of the original

resting potential. This overshoot may be of sufficient magnitude to bring the cell to the threshold for action potential firing (Solomon & Nerbonne, 1993). The differing time courses of deactivation of $I_{h,f}$ and $I_{h,s}$ may play distinct roles in controlling post-hyperpolarization 'rebound' firing. Prolonged hyperpolarizations, however, may not be required to elicit depolarizing sags and post-hyperpolarization overshoots. Periodic hyperpolarizing inputs, for example, depending on the frequency and voltage range of the induced membrane potential fluctuations, may also be able to activate $I_{h,f}$ and $I_{h,s}$. Thus, the intrinsic membrane properties of SCP neurons may amplify the effects of selected frequencies of depolarizing and hyperpolarizing inputs. In this regard, it is interesting that layer V cortical neurons have been suggested to be essential for the generation of some rhythmic field potential oscillations in *in vitro* slices (Silva, Amitai & Connors, 1991). In addition, studies in the thalamus have implicated I_h as a pacemaker for rhythmic firing (McCormick & Pape, 1990). Further work is needed to characterize the physiological roles of $I_{h,f}$ and $I_{h,s}$ in SCP neurons and to investigate their roles in the regulation of rhythmic firing in these cells.

We thank Mr John Doyle and Dr Kelleen Giffin for their excellent technical assistance in the labelling, preparation, and maintenance of cortical cultures. We also thank Drs Andreas Burkhalter, Nigel Daw, Jim Huettner, Chris Lingle and Robert Wilkinson for numerous helpful and critical discussions of this work and this manuscript. This work was supported by the National Science Foundation (BNS-8809823) and the National Institutes of Health (T32-GM07205, T32-GM07200).

REFERENCES

ANGSTADT, J. D. & CALABRESE, R. L. (1989). A hyperpolarization-activated inward current in heart interneurons of the medicinal leech. *Journal of Neuroscience* **9**, 2846–2857.

ATTWELL, D. & WILSON, M. (1980). Behaviour of the rod network in the tiger salamander retina mediated by the membrane properties of individual rods. *Journal of Physiology* **309**, 287–315.

ATTWELL, D., WERBLIN, F. S. & WILSON, M. (1982). The properties of single cones isolated from the tiger salamander retina. *Journal of Physiology* **328**, 259–283.

BEZANILLA, F. (1985). Gating of sodium and potassium channels. *Journal of Membrane Biology* **88**, 97–111.

CHAGNAC-AMITAI, Y., LUHMANN, H. J. & PRINCE, D. A. (1990). Burst generating and regular spiking layer V pyramidal neurons of rat neocortex have different morphological features. *Journal of Comparative Neurology* **296**, 598–613.

CONNORS, B. W. & GUTNICK, M. J. (1990). Intrinsic firing patterns of diverse neocortical neurons. *Trends in Neurosciences* **13**, 99–104.

CONNORS, B. W., GUTNICK, M. J. & PRINCE, D. A. (1982). Electrophysiological properties of neocortical neurons *in vitro*. *Journal of Neurophysiology* **48**, 1302–1320.

CONNORS, B. W., MALENKA, R. C. & SILVA, L. R. (1988). Two inhibitory postsynaptic potentials, and $GABA_A$ and $GABA_B$ receptor-mediated responses in neocortex of the rat and cat. *Journal of Physiology* **406**, 443–468.

DIFRANCESCO, D. (1984). Characterization of the pace-maker current kinetics in calf Purkinje fibres. *Journal of Physiology* **348**, 341–367.

DIFRANCESCO, D. & FERRONI, A. (1983). Delayed activation of the cardiac pacemaker current and its dependence on conditioning pre-hyperpolarizations. *Pflügers Archiv* **396**, 265–267.

EDMAN, Å, GESTRELIUS, S. & GRAMPP, W. (1987). Current activation by membrane hyperpolarization in the slowly adapting lobster receptor neurone. *Journal of Physiology* **384**, 671–690.

GIFFIN, K., SOLOMON, J. S., BURKHALTER, A. & NERBONNE, J. M. (1991). Differential expression of voltage-gated calcium channels in identified visual cortical neurons. *Neuron* **6**, 321–332.

HALLMAN, E. R., SCHOFIELD, B. R. & LIN, C.-S. (1988). Dendritic morphology and axon collaterals of corticotectal, corticopontine, and callosal neurons in layer V of primary visual cortex of the hooded rat. *Journal of Comparative Neurology* **272**, 149–160.

HAMILL, O. P., MARTY, A., NEHER, E., SAKMANN, B. & SIGWORTH, F. J. (1981). Improved patch-clamp techniques for high resolution current recording from cells and cell-free membrane patches. *Pflügers Archiv* **391**, 85–100.

HART, G. (1983). The kinetics and temperature dependence of the pace-maker current i_f in sheep Purkinje fibres. *Journal of Physiology* **337**, 401–416.

HESTRIN, S. (1987). The properties and function of inward rectification in rod photoreceptors of the tiger salamander. *Journal of Physiology* **390**, 319–333.

HODGKIN, A. L. & HUXLEY, A. F. (1952). A quantitative description of membrane current and its application to conduction and excitation in nerve. *Journal of Physiology* **117**, 500–544.

HORN, R. & MARTY, A. (1988). Muscarinic activation of ionic currents measured by a new whole-cell recording method. *Journal of General Physiology* **92**, 145–159.

HUETTNER, J. E. & BAUGHMAN, R. W. (1986). Primary culture of identified neurons from the visual cortex of postnatal rats. *Journal of Neuroscience* **6**, 3044–3060.

KATZ, L. C., BURKHALTER, A. & DREYER, W. J. (1984). Fluorescent latex microspheres as a retrograde neuronal marker for *in vivo* and *in vitro* studies of visual cortex. *Nature* **310**, 498–500.

KEYNES, R. D., KIMURA, J. E. & GREEFF, N. G. (1988). Kinetics of activation of the potassium conductance in the squid giant axon. *Proceedings of the Royal Society* B **232**, 375–394*P*.

LINDAU, M. & NEHER, E. (1988). Patch-clamp techniques for time-resolved capacitance measurements in single cells. *Pflügers Archiv* **411**, 137–146.

LLINAS, R. R. (1988). The intrinsic electrophysiological properties of mammalian neurons: insights into central nervous system function. *Science* **242**, 1654–1664.

MCCORMICK, D. A., CONNORS, B. W., LIGHTHALL, J. W. & PRINCE, D. A. (1985). Comparative electrophysiology of pyramidal and sparsely spiny stellate neurons of the neocortex. *Journal of Neurophysiology* **54**, 782–806.

MCCORMICK, D. A. & PAPE, H.-C. (1990). Properties of a hyperpolarization-activated cation current and its role in rhythmic oscillation in thalamic relay neurons. *Journal of Physiology* **431**, 291–318.

MASON, A. & LARKMAN, A. (1990). Correlations between morphology and electrophysiology of pyramidal neurons in slices of rat visual cortex. II. Electrophysiology. *Journal of Neuroscience* **10**, 1415–1428.

MAYER, M. L. & WESTBROOK, G. L. (1983). A voltage-clamp analysis of inward (anomalous) rectification in mouse spinal sensory ganglion neurons. *Journal of Physiology* **340**, 19–45.

NEWBERRY, N. R. & NICOLL, R. A. (1985). Comparison of the action of baclofen with γ-aminobutyric acid on rat hippocampal pyramidal cells *in vitro*. *Journal of Physiology* **360**, 161–185.

RAFF, M. C., FIELDS, K. L., HAKOMORI, S., MIRSKY, R., PRUSS, R. M. & WINTER, J. (1979). Cell type-specific markers for distinguishing and studying neurons and the major classes of glial cells in culture. *Brain Research* **174**, 283–308.

SCHOFIELD, B. R., HALLMAN, L. E. & LIN, C.-S. (1987). Morphology of corticotectal cells in the primary visual cortex of hooded rats. *Journal of Comparative Neurology* **261**, 85–97.

SILVA, L. R., AMITAI, Y. & CONNORS, B. W. (1991). Intrinsic oscillations of neocortex generated by layer 5 pyramidal neurons. *Science* **251**, 432–435.

SOLOMON, J. S. & NERBONNE, J. M. (1993). Hyperpolarization-activated currents in isolated superior colliculus projecting neurons from rat visual cortex. *Journal of Physiology* **462**, 393–420.

SPAIN, W. J., SCHWINDT, P. C. & CRILL, W. E. (1987). Anomalous rectification in neurons from cat sensorimotor cortex *in vitro*. *Journal of Neurophysiology* **57**, 1555–1576.

THONG, I. G. & DREHER, H. (1986). The development of the corticotectal pathway in the albino rat. *Developmental Brain Research* **25**, 227–238.

TYTGAT, J. & HESS, P. (1992). Evidence for cooperative interactions in potassium channel gating. *Nature* **359**, 420–423.

VAN GINNEKEN, A. C. G. & GILES, W. (1991). Voltage clamp measurements of the hyperpolarization-activated inward current I_f in single cells from rabbit sino-atrial node. *Journal of Physiology* **434**, 57–83.